Electric fields imbue enzyme reactivity by aligning active site fragment orbitals

M.E. Eberhart[a,1], **Timothy R. Wilson**[a], **T.E. Jones**[b], **and Anastassia N. Alexandrova**[c]

This manuscript was compiled on August 27, 2024

It is broadly recognized that intramolecular electric fields, produced by the protein scaffold and acting on the active site, facilitate enzymatic catalysis. This field effect can be described by several theoretical models, each of which is intuitive to varying degrees. In this contribution, we show that a fundamental effect of electric fields is to generate electrostatic potentials that facilitate the energetic alignment of reactant frontier orbitals. We apply this model to demystify the impact of electric fields on high-valent iron–oxo heme proteins: catalases, peroxidases, and peroxygenases/monooxygenases. Specifically, we show that this model easily accounts for the observed field-induced changes to the spin distribution within peroxidase active sites and explains the transition between epoxidation and hydroxylation pathways seen in Cytochrome P450 active site models. Thus, for the intuitive interpretation of the chemical effect of the field, the strategy involves analyzing the response of the orbitals of active site fragments, and their energetic alignment. We note that the energy difference between fragment orbitals involved in charge redistribution acts as a measure for the chemical hardness/softness of the reactive complex. This measure, and its sensitivity to electric fields, offers a single parameter model from which to quantitatively assess the effects of electric fields on reactivity and selectivity. Thus, the model provides an additional perspective to describe electrostatic preorganization and offer ways for its manipulation.

Electric fields | Enzyme reactivity | Frontier orbitals | Quantum mechanics | Heme proteins

Significance Statement

This work presents a physical model that explains the effects of electric fields on heme–Fe reactivity, attributing these effects to shifts in the energy levels of reactant fragment orbitals due to changes in electrostatic potential induced by the fields. This perspective offers a way to analyze and predict how electrostatic preorganization can alter an enzyme's chemistry, using the energy difference between molecular fragments to understand the corresponding charge transfer and its effect on reactivity and selectivity. The findings open a path to field engineering via sequence mutagenesis, potentially leading to new reactivity. This study enhances our understanding of enzyme reactivity, and provides a foundation for future research in enzyme engineering.

1. Introduction

Electric fields can profoundly affect chemical reactions, a fact that, while long utilized by nature in the creation of selective and efficient enzymes, was only recognized by scientists a little over fifty years ago (1). This revelation ignited the imagination of researchers, envisioning a future where tailored electric fields could be used to synthesize new molecules and materials. Indeed, advancements in synthetic methods together with theoretical developments have propelled efforts to gain the insights and tools needed to manipulate electric fields to control the chemical behavior of surfaces, biomolecules, inorganic complexes, and microporous solids, to name but a few examples (2–10). While the effects of electric fields have been discerned theoretically and experimentally, an overarching conceptual framework providing the predictive power to tailor electric fields is only now emerging (11–14). Continued growth of this framework will necessarily draw from all the common tools in the chemist's toolkit. Toward this end, it is conceptually useful to distinguish three models to account for the field induced effects on chemical reactivity.

The foundation for the first of these models is provided by electron pushing formalisms and exemplified by the research by Aragonés et al. (2). They demonstrated that an appropriately oriented external electric field (OEEF) can enhance charge transfer and lower reaction barriers. In their study of a Diels-Alder reaction, model reactants were attached to an STM break junction, which was then supplied with an OEEF. The findings indicated that the reaction was facilitated by an alignment of the electric field that promoted electron flow from the dienophile to the diene. This hypothesis was further supported by broader research concluding that catalysis could generally be enhanced by orienting an electric field in the direction of electron reorganization during the reaction (9).

The second model is an essential facet in Warshel's theory of electrostatic preorganization (15, 16). Warshel posited that the positioning of charged groups of the protein's extended structure is strategic to create local electric fields (LEFs) preorganized to reduce the energy of the transition state (TS), or in other words—align with the change of the electric dipole moment upon TS crossing. Because the field is created by the charged amino acids of the protein backbone, the entropic

Author affiliations: [a]Chemistry Department, Colorado School of Mines, 1500 Illinois Street, Golden, CO, USA; [b]Theoretical Division, Los Alamos National Laboratory, Los Alamos, New Mexico 87545, USA; [c]Department of Chemistry, and Biochemistry, University of California, Los Angeles, Los Angeles, California 90095, United States

M.E.E. conceived the study and wrote the manuscript. M.E.E. and T.R.W. performend the calculations and analysis and interpretation of results. T.E.J., and A.N.A. contributed to the interpretation of the results and the writing of the manuscript. T.R.W. created final figures and performed final document editing.

The authors declare no competing interests.

[1]To whom correspondence should be addressed. E-mail: meberhar@mines.edu

penalty for the environmental reorganization during the reaction is avoided, and the barrier to the reaction is lowered.

As an accompanying consequence, this same TS stabilizing field may, as in the Diels-Alder example above, promote the catalytic reaction's charge redistribution—further stabilizing the TS. Warshel and others (see Table 2 of Reference 16) have quantified these combined effects employing the empirical valence bond, EVB, method (17).

The third model, commonly employed by the solid-state and electrochemistry communities, is firmly rooted in frontier orbital theory. This theory underscores the significance of the relative energies of the one-electron orbitals (or bands) in the reactants and the catalyst. A pertinent example is the work of Wasileski et al. (18), who explored how the strength of the electric field affects the bonding of adsorbates to metal surfaces. They observed a correlation between the energy difference $E_f - E_a$ (E_f is the metal Fermi energy and E_a refers to the adsorbate valence energy levels) and various properties like the adsorbate's binding/adsorption energy. An applied electric field can adjust this energy difference, thereby modulating properties.

In the context of molecular systems, Model 3 dovetails with the principles of frontier orbital theory. The theory posits that reactivity is influenced by how well the energies of reactant frontier orbitals match energetically and spatially. Moreover, the energies of these one-electron orbitals can be modified, not directly by a field itself but by altering the electrostatic potential of the reactants.

First order perturbation theory is useful in making this concept more concrete. The first order correction to the energy of the i^{th} molecular orbital, ϕ_i, due to an electrostatic potential, $V_e\,(r)$, is,

$$E_i^{(1)} = \langle \phi_i | V_e(r) | \phi_i \rangle \qquad [1]$$

This correction depends only on the potential. The electric field enters the correction to the extent that it alters the potential. In the case of a uniform z oriented EEF of strength F_z, an electron will see an electrostatic potential that increases with z. The electrostatic potential experienced by an electron in such a field is given as $V_e(z) = F_z\, q_e\, z$, where q_e is the electron charge and z is a coordinate relative to some arbitrary origin. Choice of a different origin gives different values for $V_e(z)$, but the difference between the potential at two points will be unaffected.

Using this form for the potential in equation 1, yields,

$$E_i^{(1)} = -F_z \langle \phi_i | z | \phi_i \rangle = -F_z \int z\, \rho_i\, dV \qquad [2]$$

where $\rho_i = \langle \phi_i | \phi_i \rangle$ is the electron density of the i^{th} MO and the integral is taken over all space.

We will demonstrate that this third model can be used to clearly rationalize computational findings simulating the influences of OEEFs on enzyme active sites, findings that have previously been challenging to interpret. This insight serves to extend our understanding of the mechanisms underlying the catalytic activity of natural enzymes, potentially aiding in the strategic use of electric fields to enhance or suppress chemical reactions.

Our problems of interest concern high-valent iron–oxo heme proteins: e.g., catalases, peroxidases, and peroxygenases/monooxygenases (19–22). Though there are hundreds of enzymes in these three classes, they share an active moiety referred to as Compound I (Cpd I; Figure 1), which varies only in the axial ligand coordinating the heme's iron center, with tyrosine, histidine, and cysteine in the catalases, peroxidases, and peroxygenases/monooxygenases, respectively.

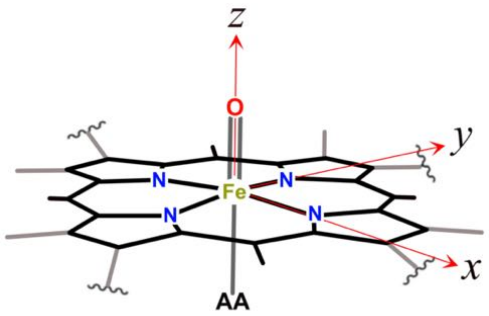

Fig. 1. Compound I: the active moiety common to catalases, peroxidases, and peroxygenases/monooxygenases. The variants of these enzymes differ in their extended structure and in the axial amino acid (AA) residue: His, Cys, or Tyr.

These enzymes generally function by oxidizing or introducing oxygen to different organic compounds, utilizing either molecular oxygen or hydrogen peroxide. In their standard state, these enzymes exist in a ferric (Fe^{III}) form with an attached water molecule, as illustrated in Scheme 1. This inactive state can be triggered through two primary routes: the first involves Fe^{III} interacting with hydrogen peroxide to produce the $(Por^{+\bullet})Fe^{IV}$=O Cpd I intermediate and water; the second pathway begins with Fe^{III} being reduced to Fe^{II}, which then binds to molecular oxygen and undergoes a series of electron and proton transfers, ultimately yielding the same Cpd I intermediate and water (23).

Cpd I is typically a triradical species with two unpaired electrons occupying orthogonal π^* antibonding orbitals of the Fe–O functionality on the heme oxygen atom and the remaining unpaired electron on the porphyrin ring or an adjacent amino acid residue (vide infra). Two nearly degenerate multiplet states have been observed, a doublet resulting from antiferromagnetic coupling between the oxygen and porphyrin radicals and a ferromagnetically coupled quartet (21).

Given the ubiquity of Cpd I across the different enzyme classes and its ability to activate strong C–H substrate bonds, attention has focused on its chemistry, which in large part is mediated by the axial ligand (24). However, equally important for reactivity control are the electric fields exerted on Cpd I by the enzyme's extended structure (excluding the heme and the axial ligand) (23). Bím and Alexandrova examined electric fields experienced by the Fe center in Cpd I in approximately 200 individual iron–oxo heme proteins and found that for all these proteins, the component of the electric field normal to the heme plane, F_z, was dominant. Furthermore, for His-ligated enzymes a strong negative (pointing from the axial oxygen ligand to the iron) F_z was observed most often while for Cys-ligated enzymes this field was exclusively positive (pointing from the iron to the axial oxygen ligand), with an average value of 28.5 MV/cm (∼0.005 au). In Tyr-ligated catalases, the fields were uniformly near zero.

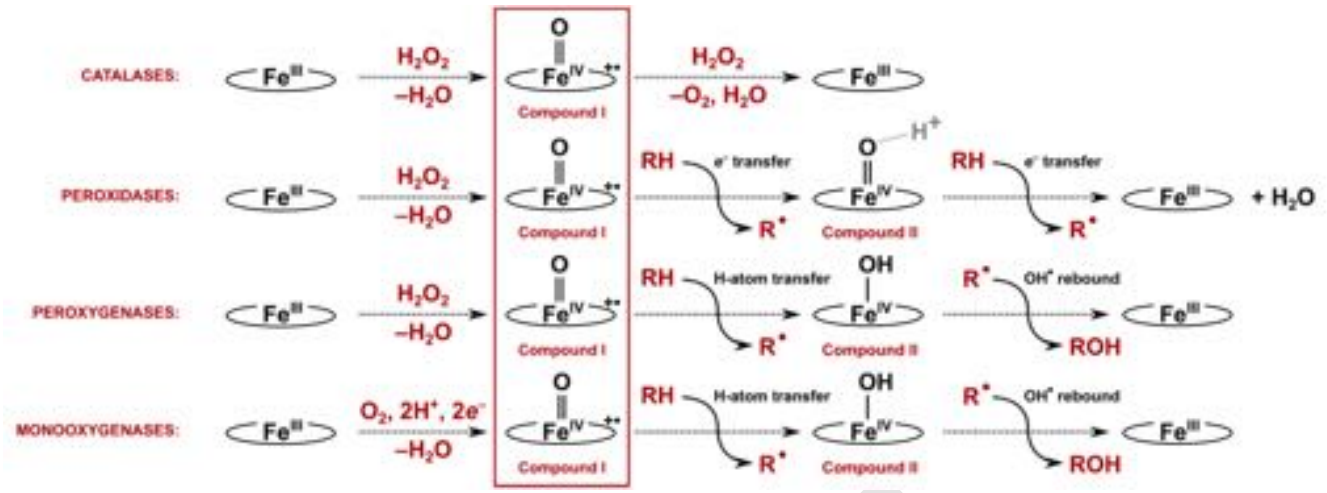

Scheme 1. Typical reactions of different classes of high-valent iron–oxo heme proteins. Adapted from Reference 23.

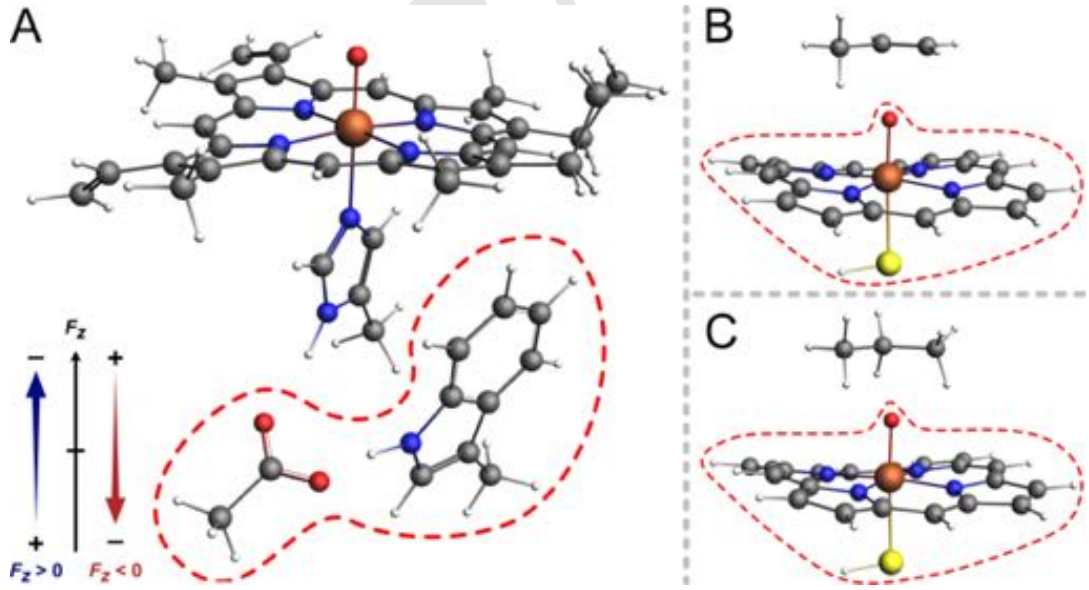

Fig. 2. The fragments decompositions of the three QM systems considered in this study. For each model, one of the two fragments is shown encircled by a dashed red line. A) Active site model of His-ligated heme enzyme with nearby residue analogues (red-dashed line); acetate representing Asp, and indole representing Trp, denoted as Asp* and Trp* respectively. B) Active site model of Cys-ligated heme enzyme with propene as the substrate. C) Active site model of Cys-ligated heme enzyme with propane as the substrate. In B and C, the heme-fragment is indicated in the red-dashed line. The field direction is aligned with the Fe–O internuclear axis with the positive direction pointing from Fe to O. Atomic coordinates for these clusters are reported in the SI.

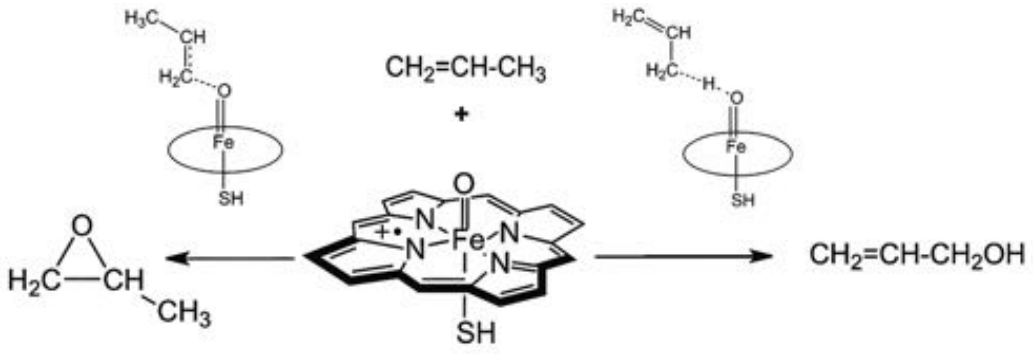

Scheme 2. Epoxidation (left) and hydroxylation (right) pathways during propene functionalization by compound I. The oxo functionality of Cpd I acts as an electrophile to activate the π-bond of propene, leading epoxidation or as a nucleophile to activate the C–H bond, leading to hydroxylation. Adapted from Reference 5

The electric fields within these enzymes may vary substantially across the active site, influenced by the substrate, local fluctuations in protein structure during the reaction, and potentially by thermal motion. Despite this variability, the observed correlations between chemical properties and the magnitude and direction of the fields at the Fe site suggest that fully understanding enzyme function necessitates a comprehensive grasp of electric field effects. To advance this understanding, researchers have developed simplified models to isolate specific aspects of these effects.

In the study of high-valent iron–oxo heme proteins, one such simplified model employs first-principles calculations on active site analogues (Figure 1) subject to an OEEF to provide a first approximation to the effects of electric field from the remainder of the enzyme's extended structure (23, 25, 26). These calculations resulted in two confounding observations.

The first of these concerns the effect of an OEEF on the unpaired electrons of His-ligated Cpd I. In the presence of a OEEF pointing from O to Fe the unpaired electron on the porphyrin will be displaced to neighboring amino acid residues. How a such a field can cause such dramatic changes in the electronic structure remains unexplained (23).

The second observation concerns Cys-ligated heme proteins, the oxygen in some of which has the remarkable ability to participate as an electrophile in epoxidation and a nucleophile in hydroxylation (27). Shaik et al. (26), using small molecule models of Cys-ligated Cpd I revealed that the selectivity between epoxidation and hydroxylation (Scheme 2) could be switched by altering the direction and magnitude of F_z. With positive values favoring epoxidation and negative values favoring hydroxylation. The authors initially noted that they could provide no straightforward explanation for these results but speculated that the effects originated from field induced state mixing.

Here we use DFT methods (see Materials and methods for more detail) to demonstrate that Model 3, which correlates orbital energy with electrostatic potential, not only clarifies these perplexing observations but also indicates a complex interaction among all three models to enhance enzyme functionality.

2. His-ligated peroxidases

The His-ligated peroxidases, for example, cytochrome c peroxidase (CcP), Leishmania major peroxidase (LmP), and ascorbate peroxidase (APX), are virtually homologous about the heme iron. In addition to their His-ligation, they share adjacent Trp and Asp residues, which together form a hydrogen bonded network that contributes to the enzyme's properties (28). The active site of these enzymes has been modeled with an analogue system shown in Figure 2A, where the His-axial ligand is replaced with imidazole while acetate and indole replace the side chains of the neighboring Asp and Trp residues (23, 25).

It should be noted that though the active site analogues across this series of peroxidases are virtually invariant, the LEF at their iron sites change. For example, the static fields computed from crystal structure data give APX $F_z = 4$ MV/cm, while for LmP and CcP $F_z = -16$ and -27 MV/cm, respectively (the field direction convention is shown in Figure 2A) (23). This variation is the result of their differing extended structures and lends support to the hypothesis that the active site LEF, and hence extended structure, plays an important role in mediating enzyme properties.

To capture the variations in electronic structure due to the differing fields, a z directed OEEF was included in the active site model of Figure 2A (23, 25). As has been mentioned, for a positive F_z one of the radicals of this triradical species was located on the porphyrin ring, but for a negative F_z this radical is displaced to the adjacent Trp and Asp residues. The ultimate factor differentiating between these two radicals awaits clarification (23).

We performed three DFT fragment calculations on the His-ligated active site model of Figure 2A with an electric field of -0.01, 0, and $+0.01$ au (-51.4, 0, and 51.4 MV/cm) applied along the z-direction. These calculations employed two fragments, as designated in Figure 2A: a His-coordinated heme, referred to as the heme-fragment, and the analogues for the Trp and Asp residues, referenced as the Asp*-Trp*-fragment. Partial correlation diagrams representing the principal interactions between fragment orbitals (FOs) to produce the frontier region active site cluster MOs are shown in Figure 3. More detailed correlation diagrams are provided as Figures S1, S2, and S3 in the SI.*

The obvious effect of the OEEF is to change the relative energies of the fragment orbitals as per Equation 2. Compared to the zero field, the negative field shifts the Asp*-Trp*-

We used both the doublet and the quartet configurations for the full Asp-Trp*-heme complex with no substantive difference to the correlation diagrams. The results shown here are for the quartet configuration.

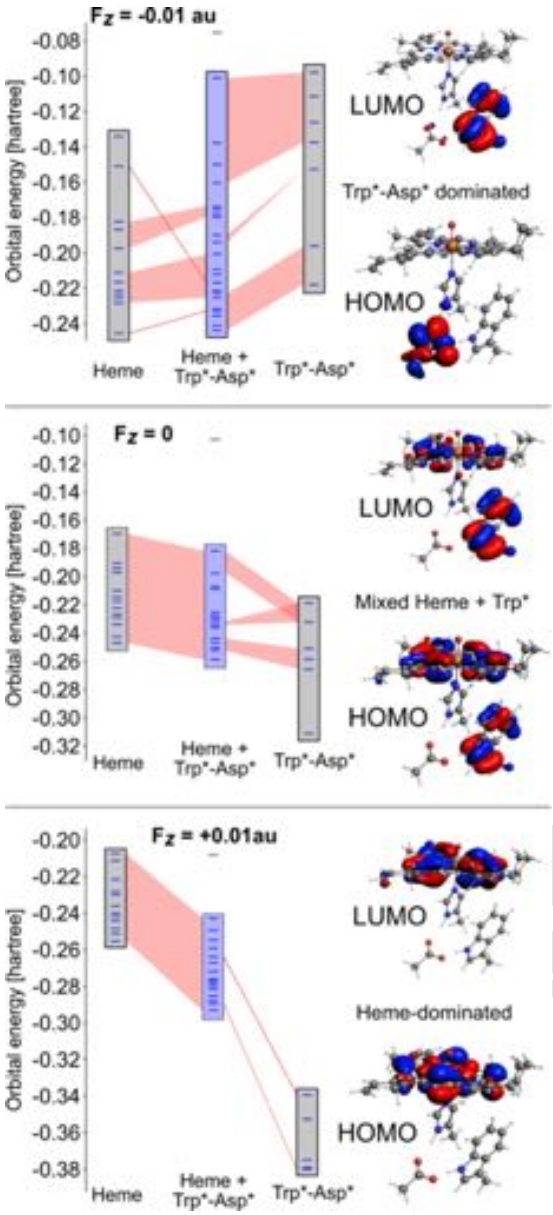

Fig. 3. Partial correlation diagrams illustrating key interactions between the Asp*-Trp*-fragment and His-ligated heme-fragment frontier orbital manifolds under a static external electric field of -0.01, 0, and $+0.01$ au (from top to bottom), and the corresponding HOMO and LUMO. In the diagrams, only occupied fragment orbitals are shown, while the LUMO is also shown for the full complex. The heme-fragment's occupied frontier orbitals create a π-complex involving S, Fe, and O atoms. The Asp*-Trp* fragment's frontier orbitals consist of the π orbitals from the acetate and indole complex. Observe the notable shifts in orbital energy levels between the heme and Asp*-Trp* fragments under the influence of the electric field, leading to changes in the active site's frontier orbital character. At a zero field (center image), these fragment orbitals mix equally, forming the Asp*-Trp*-heme complex's occupied frontier orbitals. A negative field (top image) reduces the energy levels of the heme-fragment orbitals, preventing their mixing with the Asp*-Trp*-fragment's occupied frontier orbitals. Conversely, a positive field (bottom image) results in the opposite effect.

fragment FOs significantly up in energy relative to the heme-fragment FOs, while the positive field has the opposite effect.

The consequences of these energy shifts is evident in the character of the frontier orbitals of the full active site model. Shown in Figure 3 are the LUMO and HOMO for each of the three applied electric fields. As is evident, for the negative field, shifting the energies of the Asp*-Trp* FOs up in energy leads to poor energy overlap between the frontier orbitals of the Asp*-Trp* and heme-fragments, hence the frontier orbitals of the active site cluster are now Asp*-Trp*-like. The opposite response is seen for the positive field. Accordingly, under the influence of a positive field the unpaired electron will be in heme-orbitals and under the influence of a negative field in Asp*-Trp*-orbitals.

3. Cytochrome P450 monooxygenases

We turn now to the remarkable demonstration that the selectivity between competing propene epoxidation and hydroxylation pathways could be switched by altering the direction and magnitude of an OEEF (26). Using a small molecule model system representing the Cys-ligated Cpd I of cytochrome P450 (Figure 2B), Shaik et al. calculated that an OEEF with $F_z = \pm 0.01$ au would realize a 100% selectivity toward C–H or C=C bond activation (26).

In their investigation, Shaik et al. used DFT methods to calculate the reaction path and transition state energies for both propene hydroxylation and epoxidation as catalyzed by the analogue of Cys-ligated Cpd I of Figure 2B. The rate-limiting step in each process was determined to be the activation of either the C–H or C=C bond by the oxo-group of Cpd I, resulting in the formation of an alcohol or an epoxide, respectively (Scheme 2).

In the absence of a field, the calculated transition state for epoxidation was found to be nearly degenerate with that for hydroxylation. However, for a uniform OEEF with $F_z = 0.01$ au the transition state for C–H bond activation (hydroxylation) was calculated to be 6-10 kcal/mol lower than that for C=C bond activation (epoxidation), while for $F_z = -0.01$ au the epoxidation process was calculated to be preferred by 2-6 kcal/mol.

To explain these observations, Shaik et al. investigated OEEF induced changes to the spin and charge densities of their active site model. They found that in the presence of an electric field oriented in the positive z-direction, the third unpaired electron of Cpd I is located almost entirely on the sulfur atom of the Cys analogue. When the field is reversed, most of the spin density is located on the porphyrin ring. These changes were accompanied by the transfer of about 0.3 electrons from the sulfur to the porphyrin for a positive field and the opposite for a negative applied field. Still, Shaik et al. offered no explanation for the mechanism through which these field-induced shifts to the charge density to alter the transition state energies for hydroxylation versus epoxidation; they speculated that the effects originated from field induced state mixing. Subsequently this speculation was well supported by VB modelling revealing two excited-charge transfer states. One moves electron density from propene to compound I, while the other facilitates charge transfer from sulphur towards Fe–O–propene (5).

We performed fragment calculations on a propene-Cpd I analogue shown in Figure 2B, with the propene molecule

serving as one fragment and the Cpd I analogue, referred to as the heme-fragment, as the other. Partial correlation diagrams of the near frontier orbitals for an OEEF of −0.01, 0, and +0.01 au are shown in Figure 4. (More detailed correlation diagrams are provided at Figures S4, S5, and S6 in the SI.) The HOMO and LUMO of the propene-fragment are respectively the π bonding and antibonding orbitals of the propene double bond. These FOs will shift down in energy relative to the FOs of the heme-fragment when $F_z < 0$ and up when $F_z > 0$. These shifts affect the character of the frontier orbitals of the heme-propene complex.

For $F_z > 0$, the propene HOMO is well-matched energetically with the HOMO of the heme-fragment ($\Delta E = 0.032 E_h$), promoting strong overlap. However, propene's π^* antibonding LUMO is energetically distant from the heme-fragment's HOMO ($\Delta E = 0.283 E_h$) preventing any mixing of these states. (Because these orbitals are so widely separated, we introduced discontinuities along the energy axis of Figure 4 so that the correlation between the orbitals could be depicted.) Conversely, an F_z of −0.01 au substantially reduces the energy of propene's HOMO relative to the that of the heme-fragment ($\Delta E = -0.124 E_h$), thus reducing their overlap. Simultaneously, it decreases the relative energy of propene's π^* antibonding orbital ($\Delta E = 0.126 E_h$) enough to allow it to interact with the heme-fragment's frontier orbitals. These effects are illustrated in Figure 4 with contour plots of representative frontier orbitals of the propene-heme complex. For the positive field there is no mixing between the heme-fragment MOs and the π^* antibonding orbital of propene. In the absence of a field we see a small amount of mixing in one of the complex's MOs. In the presence of a negative field, the mixing is spread across several MOs, effectively introducing electron density into propene's π^* antibonding orbital. Such electron redistribution is consistent with the Dewar-Chatt-Duncanson model (29) for C=C bond activation, offering a mechanism for epoxide formation through the application of a negative OEEF.

To better explore how a positive field facilitates C–H bond activation, we substituted the propene molecule (C–H bond dissociation energy (BDE) ∼85 kcal/mole) with propane (Figure 2C; BDE ∼100 kcal/mole) and conducted three fragment calculations with OEEFs of −0.01, 0, and +0.01 au. The corresponding partial correlation diagrams are shown in Figure 5. (Detailed correlation diagrams are shown as figures S7, S8, and S9 in the SI.)

Of note are the energies of the nearly degenerate propane-fragment H–C σ bonding HOMO and HOMO-1. In the absence of an OEEF (center pane Figure 5) these orbitals are located well below the frontier orbitals of the heme-fragment, occasioning little propane contribution to the reactive complex's frontier orbitals. The situation is exasperated in the presence of a negative field (left pane Figure 5) where propane's HOMO is so far removed from the heme-fragment frontier orbitals as to make mixing between the two negligible. However, a positive field (right pane Figure 5) brings the energy of propane's HOMO and HOMO-1 into closer alignment with the heme-fragment frontier orbitals and yields the frontier orbitals of the reactive complex to be of mixed propane-heme character. Because the z-coordinate of the heme-fragment is approximately 0, it appears to be less responsive to the OEEF than those of propane with

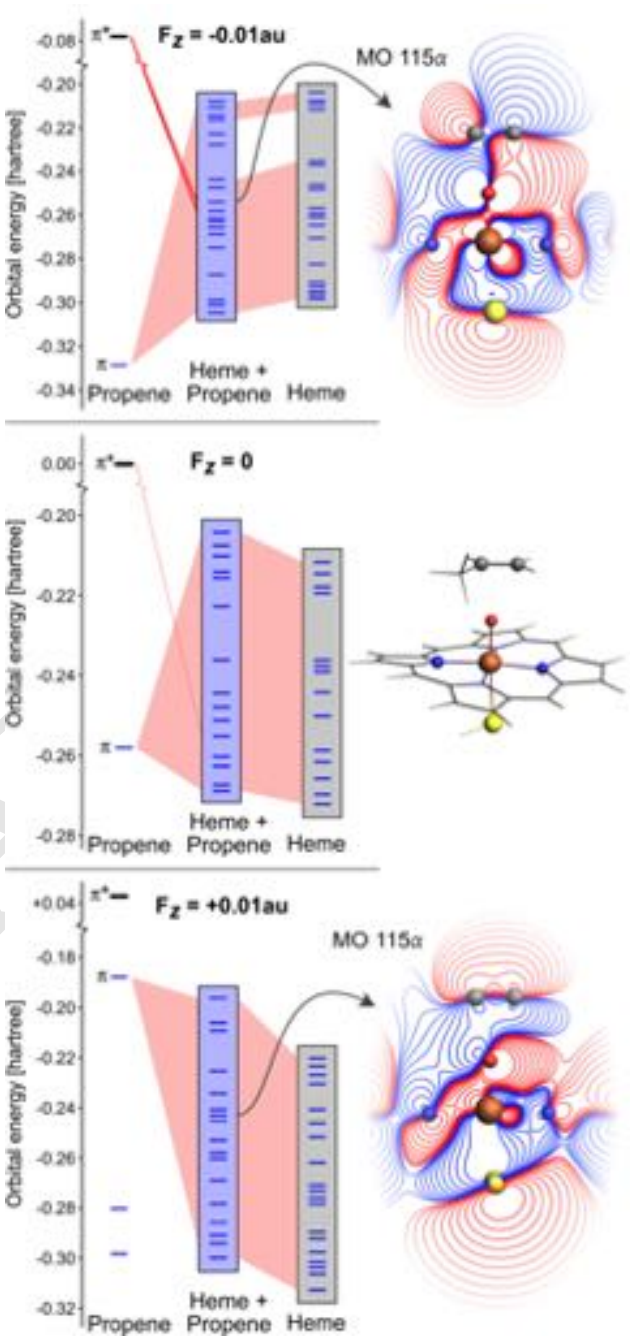

Fig. 4. Partial correlation diagrams for the interactions between the frontier regions of the propene molecule and the Cys-ligated heme analogue subjected to external electric field of (from top to bottom): −0.01, 0.00, and +0.01 au, along with contours plots in the XZ plane of representative orbitals (MO 115α) showing the mixing between the heme-fragment MOs and propene's π bonding and antibonding orbital. Note the discontinuities along the energy axes (y-axes) accounting for the large energy gaps between the propene LUMO and the rest of the MOs. The energies between the HOMO of the heme-fragment and the π^* antibonding orbital of propene are 0.0124, 0.217, and 0.251 E_h for fields of −0.01, 0, and +0.01 au respectively, while the energies between the HOMO of the heme-fragment and propene's π bonding orbital are -0.124, -0.046, and 0.032 E_h for fields of −0.01, 0, and +0.01 au respectively. For the negative field, the representative MO 115α shows propene π^* antibonding character, while for the positive field, it is characterized by π bonding character.

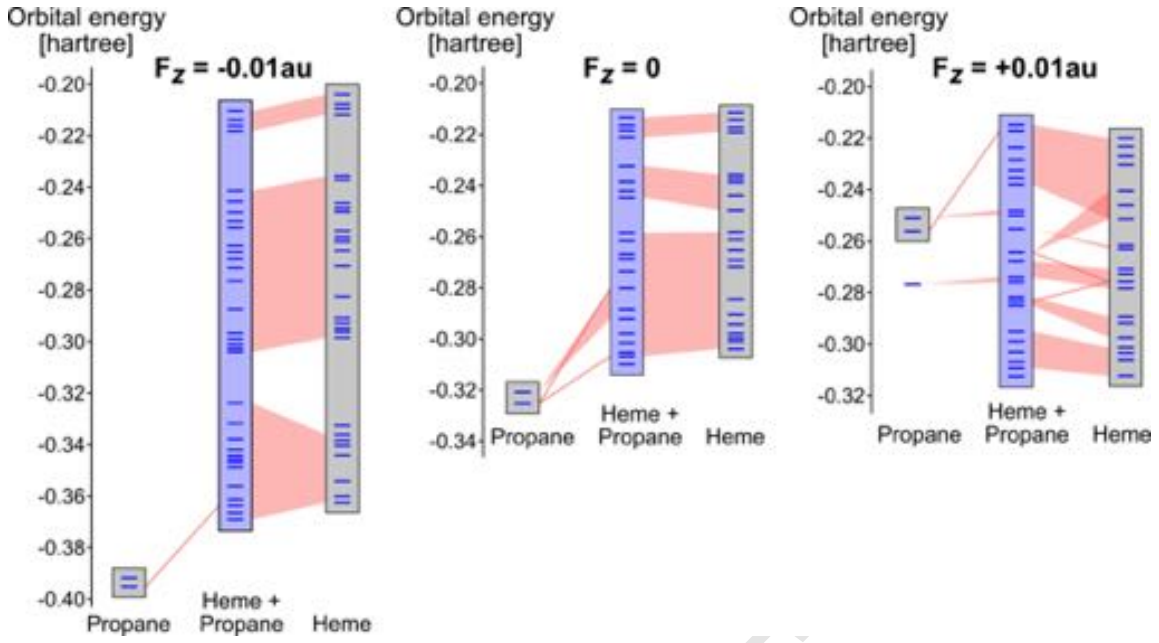

Fig. 5. Frontier molecular orbitals displaying the propane Cys-ligated heme interaction due to an applied field. The negative field depresses the energy of the occupied propane FOs to such an extent that there is little to no overlap with the heme frontier orbitals (left). With the positive field, the propane FOs are raised in energy and now mix with the heme FOs (right).

$F_z > 0$. However, had we chosen the origin to be coincident with an atom of the propane molecule, the situation would be reversed, with the heme orbitals appearing to be more responsive. The key point is that important parameter is not the field induced changes to the energies of individual MOs but the relative changes to their energies. In turn, these changes are a consequence of alterations to the electrostatic potential brought about by the electric field, whether an OEEF or a more realistic varying electric field.

We investigated the effects of the OEEF enhanced mixing by calculating the electronic structure and molecular orbital manifold along a reaction profile transferring a hydrogen atom from propane to the oxo-ligand of Cpd I to form what is known as compound II (Cpd II) and a C_3H_7 radical (Scheme 1, bottom)—the first step in the overall hydroxylation reaction.

Because the cytochrome P450 active site model shown in Figure 2A does not include a substrate pocket, our calculation is a poor representation of the reaction dynamics of the enzyme. However, our purpose was to compare the relative stabilities of the fragment configurations along the reaction profile in the presence of positive and negative applied fields.

Figure 6 shows the calculated reaction profile for an applied field of +0.01 au. A TS with an energy of ∼17 kcal/mole was found approximately 50% of the way along the reaction coordinate. (See SI for coordiantes along the reaction coordinate.) Early in the reaction the heme–propane HOMO-1 results from mixing propane's HOMO with the heme-fragment's LUMO. Later, the mixing between occupied propane FOs and unoccupied heme FOs become more intense. Where the heme–propane HOMO and HOMO-1 derive from mixing between propane's HOMO and unoccupied heme FOs. This mixing is made possible by the field induced near degeneracy of the propane and heme-fragment frontier orbitals. A situation that is intensified through the course of the reaction because propane's HOMO increases its energy

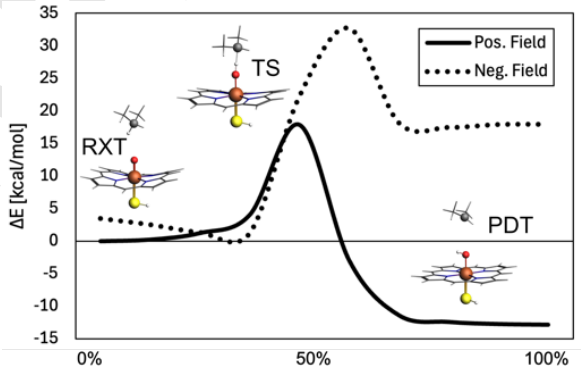

Fig. 6. The reaction profile in the presence of the +0.01 au applied field is shown (solid), as well as the corresponding profile of the same reaction path but with a −0.01 au field applied. The reactant, transition state, and product states are depicted, with important atoms emphasized. See SI for more detail.

as the H–C σ bonding interaction grows weaker. Thus, through the reaction, the energy of propane's HOMO matches increasingly well with the unoccupied heme-fragment orbitals, leading to greater overlap between propane and enzyme frontier orbitals.

Also shown in Figure 6 is the energy along the same reaction path with an applied field of −0.01 au. This path is strongly field destabilized with a maximum along the path of ∼32 kcal/mole and a positive ΔH_{rxn}. However, the configuration at this point does not represent a true TS as the negative field alters the potential energy surface. A negative field TS calculation with the same initial and final states as in Figure 6 recovers a reaction path profile qualitatively like the dotted path shown in Figure 6, again with a positive ΔH_{rxn} but with a distinct TS configuration (see SI for comparison of TS configurations). Inspection of the frontier MOs of

the heme–propane complex shows no contribution from the propane fragment orbitals, consistent with Figure 5.

The negative field lowers the energy of propane's frontier orbitals to such an extent that mixing with the unoccupied heme-fragment orbitals is not favored. Instead, propane's occupied frontier orbitals mix with occupied orbitals of the heme-fragment, minimizing the charge transfer from propane to the heme-fragment. In fact, the negative field lowers the energy of propane's unoccupied FOs sufficiently to produce a small amount of mixing with the occupied heme-fragment orbitals. This mixing, though small, leads to charge transfer from the heme-fragment to propane. The reverse direction of what is observed in the catalytic process of Scheme 1.

It is interesting to note that the HOMO-LUMO energy gaps have been associated with chemical hardness (30), where a smaller energy gap indicates greater chemical reactivity and decreased kinetic stability. If one takes the energy difference between the orbitals involved in charge transfer, e.g., propane's HOMO and the heme-fragment's LUMO, as the HOMO-LUMO energy gap for this reaction, then the application of a positive field softens the reaction and a negative field act to harden it.

4. Summary

We introduce a physical model that attributes puzzling effects of electric fields on heme–Fe reactivity to shifts in the energy levels of reactant fragment orbitals (such as heme, Trp, and reaction substrate) due to changes in electrostatic potential induced by the fields. These energy shifts depend solely on the local electrostatic potential. These shifts modify the interaction of frontier orbitals, thus enhancing or reducing reactivity. We demonstrate that significant changes in the electronic structure of His-ligated Cpd I under electric fields can be explained by the energy shifts of fragment orbitals on the Fe-heme complex and on adjacent amino acid residues. Additionally, we illustrate how the selectivity between epoxidation and hydroxylation in Cys-ligated Cpd I is influenced by field-induced variations in the energy of fragment orbitals from the Cys-ligated Fe–heme and the reacting substrate. Further, we hypothesize that the energy difference between fragment orbitals involved in inter-fragment charge transfer may quantitatively evaluate the impact of electric fields on reactivity and selectivity.

These findings support the hypothesis that one role of an enzyme's internally generated electric field is to modify the electrostatic potential at crucial active site locations, thereby enhancing the energy alignment between the frontier orbitals of the catalyst and the reactants. However, there are countless electric fields that could produce the same electrostatic potential at these key points. Each of these distinct fields would interact with the active site electron density in a unique fashion. A subset of these fields would accelerate the catalytic reaction's electron reorganization in accordance with Model 1. Of these, consistent with the theory of electrostatic preorganization, some fields would simultaneously align polar and charged groups to further lower TS energy. Thus, Nature faces an optimization challenge: choosing between an electric field that optimizes the energies of reactant orbitals and one that facilitates charge redistribution and transition state stabilization. While it's possible that the fields best suited for promoting charge redistribution also maximize orbital energy overlap, we believe it is more likely that an enzyme's complex electric field is the product of Nature's attempt to balance these two effects. Understanding how Nature resolves this balancing act will be crucial to the developing discipline of electric field design. Further research into the topology and geometry of electrostatic potentials in different enzymes and catalysts will be necessary to uncover the answer to this mystery.

Materials and Methods

We reprised the referenced calculations in Section 1 using the Amsterdam Density Functional (ADF) package (31, 32). For these calculations we used the B3LYP hybrid functional (33) with an all-electron triple zeta with polarization Slater-type-orbital basis set (34, 35). We used the same active analogues as those employed in reference 23 and 26 and shown in Figure 2. The active site analogues of the heme group were allowed to relax in response to the applied field. In addition, we took advantage of ADF's fragment orbital capability in which molecular orbitals are expanded as a linear combination of the orbitals of predefined molecular fragments, so-called fragment orbitals (FOs). Presenting the results in the form of fragment correlation diagrams provides the ideal visual tool to assess the effects of varying electrostatic potential on the electronic structures of the Cpd I analogues.

Data, Materials, and Software Availability

The SI contains the atomic coordinates of the active site analogues used in this study.

ACKNOWLEDGMENTS. This work was supported by the NSF-CHE grant 2203366 grant to A.N.A. and M.E.E. M.E.E. and T.W. acknowledge the support of the State of Colorado AIA 2021 grant.

Reviewer comments

1. Y Pocker, RF Buchholz, Electrostatic catalysis of ionic aggregates. I. Ionization and dissociation of trityl chloride and hydrogen chloride in lithium perchlorate-diethyl ether solutions. *J. Am. Chem. Soc.* **92**, 2075–2084 (1970).
2. AC Aragonès, et al., Electrostatic catalysis of a Diels–Alder reaction. *Nature* **531**, 88–91 (2016).
3. WY Kim, KS Kim, Tuning Molecular Orbitals in Molecular Electronics and Spintronics. *Accounts Chem. Res.* **43**, 111–120 (2010).
4. S Shaik, D Mandal, R Ramanan, Oriented electric fields as future smart reagents in chemistry. *Nat. Chem.* **8**, 1091–1098 (2016).
5. S Shaik, R Ramanan, D Danovich, D Mandal, Structure and reactivity/selectivity control by oriented-external electric fields. *Chem. Soc. Rev.* **47**, 5125–5145 (2018).
6. S Ciampi, N Darwish, HM Aitken, I Díez-Pérez, ML Coote, Harnessing electrostatic catalysis in single molecule, electrochemical and chemical systems: A rapidly growing experimental tool box. *Chem. Soc. Rev.* **47**, 5146–5164 (2018).
7. AM Thayer, Drug Repurposing. *Chem. & Eng. News* **90** (2012).
8. DK Ro, et al., Production of the antimalarial drug precursor artemisinic acid in engineered yeast. *Nature* **440**, 940–943 (2006).
9. T Stuyver, D Danovich, J Joy, S Shaik, External electric field effects on chemical structure and reactivity. *WIREs Comput. Mol. Sci.* **10**, e1438 (2020).
10. C Zheng, et al., A two-directional vibrational probe reveals different electric field orientations in solution and an enzyme active site. *Nat. Chem.* **14**, 891–897 (2022).
11. X Zhao, et al., Designing a Built-In Electric Field for Efficient Energy Electrocatalysis. *ACS Nano* **16**, 19959–19979 (2022).
12. SA Siddiqui, T Stuyver, S Shaik, KD Dubey, Designed Local Electric Fields-Promising Tools for Enzyme Engineering. *JACS Au* **3**, 3259–3269 (2023).
13. AB Weberg, RP Murphy, NC Tomson, Oriented internal electrostatic fields: An emerging design element in coordination chemistry and catalysis. *Chem. Sci.* **13**, 5432–5446 (2022).
14. VV Welborn, L Ruiz Pestana, T Head-Gordon, Computational optimization of electric fields for better catalysis design. *Nat. Catal.* **1**, 649–655 (2018).
15. A Warshel, Electrostatic origin of the catalytic power of enzymes and the role of preorganized active sites. *The J. Biol. Chem.* **273**, 27035–27038 (1998).
16. A Warshel, et al., Electrostatic Basis for Enzyme Catalysis. *Chem. Rev.* **106**, 3210–3235 (2006).
17. A Warshel, RM Weiss, An empirical valence bond approach for comparing reactions in solutions and in enzymes. *J. Am. Chem. Soc.* **102**, 6218–6226 (1980).
18. SA Wasileski, MTM Koper, MJ Weaver, Field-Dependent Electrode-Chemisorbate Bonding: Sensitivity of Vibrational Stark Effect and Binding Energetics to Nature of Surface Coordination. *J. Am. Chem. Soc.* **124**, 2796–2805 (2002).
19. X Huang, JT Groves, Oxygen Activation and Radical Transformations in Heme Proteins and Metalloporphyrins. *Chem. Rev.* **118**, 2491–2553 (2018).
20. PCE Moody, EL Raven, The Nature and Reactivity of Ferryl Heme in Compounds I and II. *Accounts Chem. Res.* **51**, 427–435 (2018).
21. TL Poulos, Heme Enzyme Structure and Function. *Chem. Rev.* **114**, 3919–3962 (2014).
22. M Sono, MP Roach, ED Coulter, JH Dawson, Heme-Containing Oxygenases. *Chem. Rev.* **96**, 2841–2888 (1996).
23. D Bím, AN Alexandrova, Local Electric Fields As a Natural Switch of Heme-Iron Protein Reactivity. *ACS Catal.* **11**, 6534–6546 (2021).
24. D Balcells, C Raynaud, RH Crabtree, O Eisenstein, A Rational Basis for the Axial Ligand Effect in C-H Oxidation by [MnO(porphyrin)(X)]+ (X = H2O, OH-, O2-) from a DFT Study. *Inorg. Chem.* **47**, 10090–10099 (2008).
25. SP de Visser, What Affects the Quartet-Doublet Energy Splitting in Peroxidase Enzymes? *The J. Phys. Chem. A* **109**, 11050–11057 (2005).
26. S Shaik, SP de Visser, D Kumar, External Electric Field Will Control the Selectivity of Enzymatic-Like Bond Activations. *J. Am. Chem. Soc.* **126**, 11746–11749 (2004).
27. RB Grant, RM Lambert, A single crystal study of the silver-catalysed selective oxidation and total oxidation of ethylene. *J. Catal.* **92**, 364–375 (1985).
28. DB Goodin, DE McRee, The Asp-His-iron triad of cytochrome c peroxidase controls the reduction potential electronic structure, and coupling of the tryptophan free radical to the heme. *Biochemistry* **32**, 3313–3324 (1993).
29. J Chatt, LA Duncanson, LM Venanzi, Directing effects in inorganic substitution reactions. Part I. A hypothesis to explain the trans-effect. *J. Chem. Soc. (Resumed)* pp. 4456–4460 (1955).
30. RG Pearson, Hard and soft acids and bases—the evolution of a chemical concept. *Coord. Chem. Rev.* **100**, 403–425 (1990).
31. G te Velde, et al., Chemistry with ADF. *J. Comput. Chem.* **22**, 931–967 (2001).
32. C Fonseca Guerra, JG Snijders, G te Velde, EJ Baerends, Towards an order-N DFT method. *Theor. Chem. Accounts* **99**, 391–403 (1998).
33. PJ Stephens, FJ Devlin, CF Chabalowski, MJ Frisch, Ab Initio Calculation of Vibrational Absorption and Circular Dichroism Spectra Using Density Functional Force Fields. *The J. Phys. Chem.* **98**, 11623–11627 (1994).
34. CW Bauschlicher, H Partridge, A comparison of correlation-consistent and Pople-type basis sets. *Chem. Phys. Lett.* **245**, 158–164 (1995).
35. E Van Lenthe, EJ Baerends, Optimized Slater-type basis sets for the elements 1–118. *J. Comput. Chem.* **24**, 1142–1156 (2003).